Chapter 2

Near Fields of Wire Antennas

In this section, the matrix methods are used for the computation of current distribution on a half-wave dipole antenna and the computation of near-field distributions from the current distributions on the wire antenna.

It is assumed here that the wire is thin, i.e., the radius of the wire is significantly smaller than both the wavelength and the length of the wire. This assumption of a "thin wire" simplifies the analysis as it only takes into account currents that flow along the axis of the wire. As a result, there is no consideration of currents directed azimuthally or circumferentially around the wire. To approximate current and charge densities, filaments of current and charge along the axis of the wire are used. The boundary condition concerning the tangential component of the electric field at the wire surfaces is approximately satisfied by requiring that the axial component vanishes at the surface of each wire. In the subsectional approach used, the wire is considered as N short segments connected together. The endpoints of each segment define a pair of terminals in space. If we consider that these N pairs of

terminals form an N port network, then the wire object can be obtained by short-circuiting all ports of the network. The impedance matrix of the N port network can be determined by applying a current source to each port and calculating the open circuit voltage at all ports. This procedure involves only current elements in free space. Once the impedance matrix is obtained, the admittance matrix can be found by inversion of the impedance matrix. The current distribution for any particular voltage excitation is then obtained by matrix multiplication of the voltage with the admittance matrix.

An integral equation for the charge density σ_s, and current $\mathbf{J_s}$ on a conducting body S in a known impressed field $\mathbf{E^i}$ is obtained as follows. The scattered field $\mathbf{E^s}$, produced by σ_s and $\mathbf{J_s}$, is expressed in terms of retarded potential integrals. The boundary condition $\hat{\mathbf{n}} \times (\mathbf{E^i} + \mathbf{E^s}) = 0$ on S is applied. This is summarized by

$$\mathbf{E^s} = -j\omega\mathbf{A} - \nabla\phi \tag{2.1}$$

$$\mathbf{A} = \mu \oiint_S \mathbf{J_s} \frac{e^{-jkR}}{4\pi R} dS \tag{2.2}$$

$$\phi = \frac{1}{\varepsilon} \oiint_S \sigma_s \frac{e^{-jkR}}{4\pi R} dS \tag{2.3}$$

$$\sigma_s = -\frac{1}{j\omega} \nabla_s \cdot \mathbf{J_s} \tag{2.4}$$

$$\hat{\mathbf{n}} \times \mathbf{E^s} = -\hat{\mathbf{n}} \times \mathbf{E^i} \tag{2.5}$$

An arbitrary thin-wire antenna is depicted in Fig. 2.1(a). The approximations made for the computation of the current distribution of the wire antenna are as follows:

(a) The current flows only in the axial direction.

(a) (b)

Fig. 2.1: (a) A Wire Antenna (b) The Wire axis divided by N segments [8]

(b) The current and charge densities are approximated by filaments of current $\mathbf{I}$ and charge σ on the wire axis.

(c) The boundary condition (2.5) is applied only to the axial component of $\mathbf{E}$ at the wire surface.

According to this approximation, (2.1) to (2.5) become

$$-E_l^i = -j\omega A_l - \frac{\partial \phi}{\partial l} \qquad \text{on } S \tag{2.6}$$

$$\mathbf{A} = \mu \int_{axis} \mathbf{I}(l) \frac{e^{-jkR}}{4\pi R} dl \tag{2.7}$$

$$\phi = \frac{1}{\varepsilon} \int_{axis} \sigma(l) \frac{e^{-jkR}}{4\pi R} dl \tag{2.8}$$

$$\sigma = -\frac{1}{j\omega} \frac{dI}{dl} \tag{2.9}$$

where l is the length variable along the wire axis and R is measured from a source point on the axis to a field point on the wire surface. The integrals are approximated

as the sum of integrals over N small segments, obtained by treating I and q as constant over each segment. Derivatives are approximated by finite differences over the same intervals used for integration. Fig. 2.1(b) illustrates the division of the wire axis into N segments. The boundary condition $I = 0$ is taken into account by starting the first segment half interval inside from the end of the wire. The nth segment is identified by its starting point $\bar{n}$, its midpoint n, and its termination $\overset{+}{n}$. An increment Δl_n denotes that between $\bar{n}$ and $\overset{+}{n}$. Δl_n^- and Δl_n^+ denote increments shifted half segments minus or plus along l. The desired approximations for (2.6) to (2.9) are then

$$-E_l^i(m) \approx -j\omega A_l(m) - \frac{\phi(\overset{+}{m}) - \phi(\bar{m})}{\Delta l_m} \tag{2.10}$$

$$\mathbf{A}(m) = \mu \sum_n \mathbf{I}(n) \int_{\Delta l_n} \frac{e^{-jkR}}{4\pi R} dl \tag{2.11}$$

$$\phi(\overset{+}{m}) \approx \frac{1}{\varepsilon} \sum_n \sigma(\overset{+}{n}) \int_{\Delta l_{\overset{+}{n}}} \frac{e^{-jkR}}{4\pi R} dl \tag{2.12}$$

$$\phi(\bar{m}) \approx \frac{1}{\varepsilon} \sum_n \sigma(\bar{n}) \int_{\Delta l_{\bar{n}}} \frac{e^{-jkR}}{4\pi R} dl \tag{2.13}$$

$$\sigma(\overset{+}{n}) \approx -\frac{1}{j\omega} \left[\frac{I(n+1) - I(n)}{\Delta l_{\overset{+}{n}}} \right] \tag{2.14}$$

$$\sigma(\bar{n}) \approx -\frac{1}{j\omega} \left[\frac{I(n) - I(n-1)}{\Delta l_{\bar{n}}} \right] \tag{2.15}$$

Equations (2.10) through (2.15) are applied to two isolated elements, and the impedance matrix is obtained directly.

Let us consider two representative elements of the wire antenna, as shown in Fig. 2.2. The integrals in equations (2.11) to (2.13) have the same form. So, they are

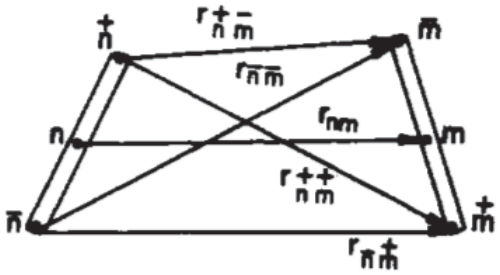

Fig. 2.2: Two Segments of a Wire Antenna [8]

denoted by

$$\psi(n,m) = \frac{1}{\Delta l_n} \int_{\Delta l_n} \frac{e^{-jkR_{mn}}}{4\pi R_{mn}} dl_n \tag{2.16}$$

Symbols '+' and '−' are used over m and n when appropriate.

Let element n of Fig. 2.2 consist of a current filament $I(n)$, and two charge filaments of net charge

$$q(\overset{+}{n}) = \frac{1}{j\omega} I(n) \qquad\qquad q(\overset{-}{n}) = -\frac{1}{j\omega} I(n) \tag{2.17}$$

where $q = \sigma \Delta l$.

The vector potential at m due to $I(n)$ is, by (2.11),

$$\mathbf{A} = \mu \mathbf{I}(n) \Delta l_n \psi(n,m) \tag{2.18}$$

The scalar potentials at $\overset{+}{m}$ and $\overset{-}{m}$ due to charges (2.17) are, by (2.12) and (2.13)

$$\begin{aligned} \phi(\overset{+}{m}) &= \frac{1}{j\omega\varepsilon} \left[I(n)\psi(\overset{+}{n},\overset{+}{m}) - I(n)\psi(\overset{-}{n},\overset{+}{m}) \right] \\ \phi(\overset{-}{m}) &= \frac{1}{j\omega\varepsilon} \left[I(n)\psi(\overset{+}{n},\overset{-}{m}) - I(n)\psi(\overset{-}{n},\overset{-}{m}) \right] \end{aligned} \tag{2.19}$$

Substituting from (2.18) and (2.19) to (2.10), and forming $Z_{mn} = \mathbf{E}^i(m) \cdot \Delta l_m / I(n)$,

we get

$$Z_{mn} = j\omega\mu\Delta l_n \cdot \Delta l_m \psi(n,m) + \frac{1}{j\omega\varepsilon}[\psi(\overset{+}{n},\overset{+}{m}) - \psi(\overset{-}{n},\overset{+}{m}) - \psi(\overset{+}{n},\overset{-}{m}) + \psi(\overset{-}{n},\overset{-}{m})] \tag{2.20}$$

Equation (2.10) can be written in Matrix form

$$[V] = [Z][I] \tag{2.21}$$

by defining

$$[I] = \begin{bmatrix} I(1) \\ I(2) \\ \vdots \\ I(N) \end{bmatrix} \qquad [V] = \begin{bmatrix} \mathbf{E}^i(1) \cdot \mathbf{l}_1 \\ \mathbf{E}^i(2) \cdot \mathbf{l}_2 \\ \vdots \\ \mathbf{E}^i(N) \cdot \mathbf{l}_N \end{bmatrix} \tag{2.22}$$

The elements of $[Z]$ matrix can be obtained from (2.20).

A wire antenna is obtained when the wire is excited by a voltage source at one or more points along its length. Hence, for an antenna excited in the nth interval, the applied voltage matrix (2.22) is

$$[V^s] = \begin{bmatrix} 0 \\ \vdots \\ V_n \\ \vdots \\ 0 \end{bmatrix} \tag{2.23}$$

i.e., all elements are zero except the nth, which is equal to the source voltage. The current distribution is given by

$$[I] = V_n \begin{bmatrix} Y_{1n} \\ Y_{2n} \\ \vdots \\ Y_{Nn} \end{bmatrix} \tag{2.24}$$

where $[Y] = [Z]^{-1}$.

Once the current distribution is known, input impedances for specific feed points and various far-field patterns of interest can be computed using standard formulas in the conventional manner [9–11]. However, it's important to note that an additional step or procedure is necessary for the computation of most near-field distributions. The description provided in [12] outlines two procedures, both derived from equation (2.21), which are programmed.

2.1 Method 1: Procedure based on Reciprocity

By the reciprocity theorem,

$$\int_v \mathbf{E_1} \cdot \mathbf{J_2}\, dv = \int_v \mathbf{E_2} \cdot \mathbf{J_1} dv \tag{2.25}$$

In the equation provided, $\mathbf{J_1}$ and $\mathbf{J_2}$ represent the source current densities, while $\mathbf{E_1}$ and $\mathbf{E_2}$ correspond to the electric fields associated with these sources. It is convenient to regard $\mathbf{J_1}$ as the known current distribution on the structure and $\mathbf{J_2}$ as the current of an infinitesimal testing dipole positioned at the field point under

consideration, aligned in the direction of the desired field component. It is assumed that the current within each wire flows exclusively in its axial direction. If we denote the wire structure as l_1 and the testing dipole as l_2, then equation (2.25) can be expressed as:

$$\int_{l_2} \mathbf{E_1} \cdot I_2 \, d\mathbf{l_2} = \int_{l_1} \mathbf{E_2} \cdot I_1 d\mathbf{l_1} \tag{2.26}$$

In this context, I_1 and I_2 represent axial currents, with their respective directions indicated by $d\mathbf{l_1}$ and $d\mathbf{l_2}$. For the infinitesimal dipole, I_2 is considered constant over l_2 as $l_2 \to 0$. Consequently, equation (2.26) can be simplified as:

$$(E_1)_{\text{along } l_2} = \frac{1}{I_2 l_2} \int_{l_1} \mathbf{E_2} \cdot I_1 d\mathbf{l_1} \tag{2.27}$$

The current I_1 is known, and $\mathbf{E_2}$, the field generated by the infinitesimal dipole, can be readily computed. Therefore, equation (2.27) serves as a valuable starting point from which the desired field components can be determined.

$\mathbf{E_2}$ can be calculated by employing the vector and scalar potentials as follows:

$$\mathbf{E_2} = -j\omega\mu\mathbf{A_2} - \nabla\phi_2 \tag{2.28}$$

where [11]

$$\mathbf{A_2} = \frac{I_2 l_2}{4\pi R} e^{-jkR} \tag{2.29}$$

$$\phi_2 = -\frac{1}{j\omega\varepsilon} \nabla \cdot \mathbf{A_2} = \frac{I_2 \, e^{-jkR}}{4\pi j\omega\varepsilon R} \left[\frac{1}{R} + jk\right] \mathbf{l_2} \cdot \hat{R} \tag{2.30}$$

and where $k = 2\pi/\lambda$. R is the distance from the testing dipole to a point on l_1, and $\hat{R}$

is its associated unit vector. Substituting (2.28) into (2.27) and integrating by parts yields

$$(E_1)_{\text{along } l_2} = \frac{1}{I_2 l_2}\left[-j\omega\mu \int_{l_1} I_1 \mathbf{A_2}\cdot d\mathbf{l_1} + \int_{l_1} \phi_2 \frac{dI_1}{dl_1} dl_1\right] \tag{2.31}$$

where the fact that the current becomes zero at the open ends of the wires is taken into account.

The piecewise linear approximation or triangle function is the current expansion selected for use with this procedure. Triangle functions are also used as testing functions, resulting in a Galerkin solution. In this case, the expansion can be written as

$$I_1 = \sum_{n=1}^{N} I'_n T_n \tag{2.32}$$

where T_n is the nth triangle expansion function, I'_n is complex amplitude, and N is the total number of expansion functions of current. Inserting (2.32) in (2.31) results in

$$(E_1)_{\text{along } l_2} = \frac{1}{I_2 l_2}\left[-j\omega\mu \sum_{n=1}^{N} \int_{l_1} I'_n T_n \mathbf{A_2}\cdot d\mathbf{l_1} + \sum_{n=1}^{N} \int_{l_1} \phi_2 I'_n \frac{dT_n}{dl_1} dl_1\right] \tag{2.33}$$

If we consider a z-directed testing dipole, then (2.33) reduces to

$$\begin{aligned}(E_{1z})_{\text{along } l_2} = \frac{1}{4\pi j\omega\varepsilon}\Bigg[&k^2 \sum_{n=1}^{N} I'_n \int_{l_1} T_n \frac{e^{-jkR}}{R} dz' \\ &+ \sum_{n=1}^{N} I'_n \int_{l_1} \frac{e^{-jkR}}{R}\left(\frac{1}{R^2} + \frac{j\omega}{R}\right)(z-z')\frac{dT_n}{dz'} dz'\Bigg]\end{aligned} \tag{2.34}$$

For electric fields along the x and y-directions respectively, (2.33) becomes

$$(E_{1x})_{\text{along } l_2} = \frac{1}{4\pi j\omega\varepsilon}\left[\sum_{n=1}^{N} I'_n \int_{l_1} \frac{e^{-jkR}}{R}\left(\frac{1}{R^2}+\frac{j\omega}{R}\right)(x-x')\frac{dT_n}{dz'}dz'\right] \quad (2.35)$$

and

$$(E_{1y})_{\text{along } l_2} = \frac{1}{4\pi j\omega\varepsilon}\left[\sum_{n=1}^{N} I'_n \int_{l_1} \frac{e^{-jkR}}{R}\left(\frac{1}{R^2}+\frac{j\omega}{R}\right)(y-y')\frac{dT_n}{dz'}dz'\right] \quad (2.36)$$

The electric field components (in cylindrical coordinates), E_z and E_ρ are obtained using (2.34), (2.35), and (2.36) and the results are shown in Fig. 2.4.

2.2 Method 2: Alternative Procedure

If we approximate the current of the given wire structure using a total of N expansion functions, then equation (2.21) simply represents:

$$\begin{bmatrix} V_1 \\ V_2 \\ \vdots \\ V_N \end{bmatrix} = \begin{bmatrix} z_{11} & z_{12} & \cdots & z_{1N} \\ z_{21} & z_{22} & \cdots & z_{2N} \\ \vdots & \vdots & \vdots & \\ z_{N1} & z_{N2} & \cdots & z_{NN} \end{bmatrix} \begin{bmatrix} I_1 \\ I_2 \\ \vdots \\ I_N \end{bmatrix} \quad (2.37)$$

To evaluate the electric field at a particular point in the near field, a small testing thin-wire dipole can be positioned at that point, aligned parallel to the relevant vector component. An additional expansion function is introduced for this testing wire, increasing the total to $N+1$ functions. As a result, the system is described by

an expanded Z matrix given as

$$\begin{bmatrix} V_1 \\ V_2 \\ \vdots \\ V_{N+1} \end{bmatrix} = \begin{bmatrix} z_{11} & z_{12} & \cdots & z_{1(N+1)} \\ z_{21} & z_{22} & \cdots & z_{2(N+1)} \\ \vdots & \vdots & \vdots & \\ z_{(N+1)1} & z_{(N+1)2} & \cdots & z_{(N+1)(N+1)} \end{bmatrix} \begin{bmatrix} I_1 \\ I_2 \\ \vdots \\ I_{N+1} \end{bmatrix} \tag{2.38}$$

If the testing wire is open-circuited then $I_{N+1} = 0$ so that

$$V_{N+1} = z_{(N+1)1} I_1 + z_{(N+1)2} I_2 + z_{(N+1)N} I_N \tag{2.39}$$

Knowledge of the current distribution along the wire structure and having an extra row in the impedance matrix that accounts for mutual impedances between the wire structure and the testing dipole allows for the calculation of the open-circuit voltage at the testing port. The electric field strength in the direction represented by the unit vector $\hat{l}$ can be expressed as:

$$E_{\text{along } \hat{l}} = \frac{-(V_{N+1}) \text{ open circuit}}{\text{length of testing dipole}} \tag{2.40}$$

As before, the approach for computing near fields involves evaluating equation (2.40) separately for each electric field vector component of interest at each specific point. The results presented here are obtained using a testing dipole with a length of 0.001λ.

It's important to emphasize that in both methods for computing near fields, the current distribution of the actual antenna is calculated without considering the presence

of the testing element used for field sampling. In the case of the second method, this means that the impedance matrix described in equation (2.37) is inverted to derive the antenna current rather than using the extended matrix as shown in equation (2.38). The last row of the matrix in equation (2.38) is specifically computed and employed to calculate only one component of the near field at a given point. Therefore, this row must be recalculated for each component at every point of interest. The fact that near-field results are essentially unaffected by the specific testing wire used is evident from the absence of the self-impedance term $z_{(N+1)(N+1)}$ in equation (2.39). This second method is implemented using the staircase current approximation and a point-matching solution.

2.3 Results and Observation

Fig. 2.3 illustrates the current distribution on a center-fed, half-wavelength dipole with a radius of 0.005λ. The wavelength is assumed to be 1 meter in this case. This result is obtained using $N = 32$ subsections. Using this current distribution of the half-wave dipole antenna, the near fields of the same antenna are calculated. Fig. 2.4 illustrates the computed electric near fields of a center-fed half-wavelength

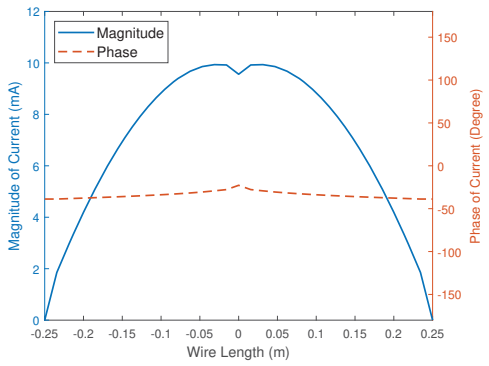

Fig. 2.3: Current distribution on a center-fed half-wave dipole (radius$= 0.005\lambda$)

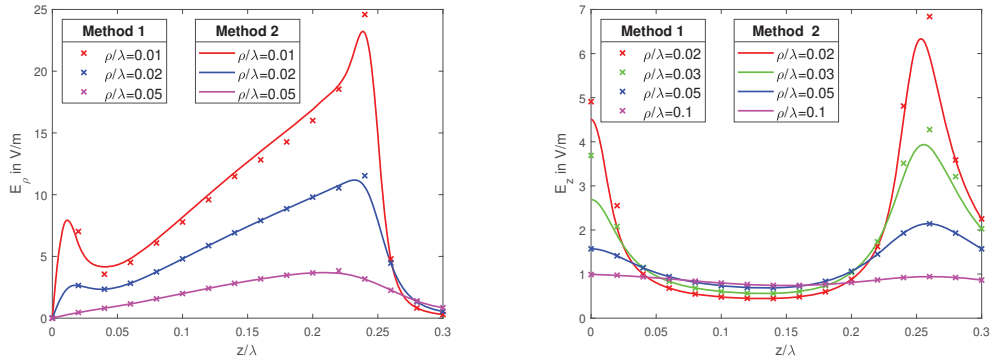

(a) (b)

Fig. 2.4: Magnitude Plot for Near fields of a center-fed half dipole (radius = 0.005λ) using Method 1 and Method 2 (a) E_ρ w.r.t. z/λ (b) E_z w.r.t. z/λ

dipole using both the methods mentioned above. Fig. 2.4(a) shows the radial fields E_ρ computed for ρ/λ values, 0.01, 0.02, and 0.05 and Fig. 2.4(b) illustrates the tangential fields E_z components, computed for ρ/λ values, 0.02, 0.03, 0.05, and 0.1. The ρ/λ values are chosen in this manner in order to compare the results with those given in [12]. The results obtained by using Method 1 and Method 2 are very close to each other, and they also match the results shown in [12] to a great extent. A comparison of the computed results with the results given in [12] is shown in Fig. 2.5.

It can be observed that the radial field E_ρ predominates across the majority of the displayed region in the figure. E_ρ exhibits peaks in proximity to the gap and the ends, with even higher peaks at the ends themselves. In the region situated halfway between the gap and the ends, $\partial E_z/\partial z$ is nearly zero and, therefore, E_ρ has approximately a $(1/\rho)$ dependence.

The tangential component E_z is small except in the gap region and near the ends of the antenna. The fields near the ends are greater than those near the gap region,

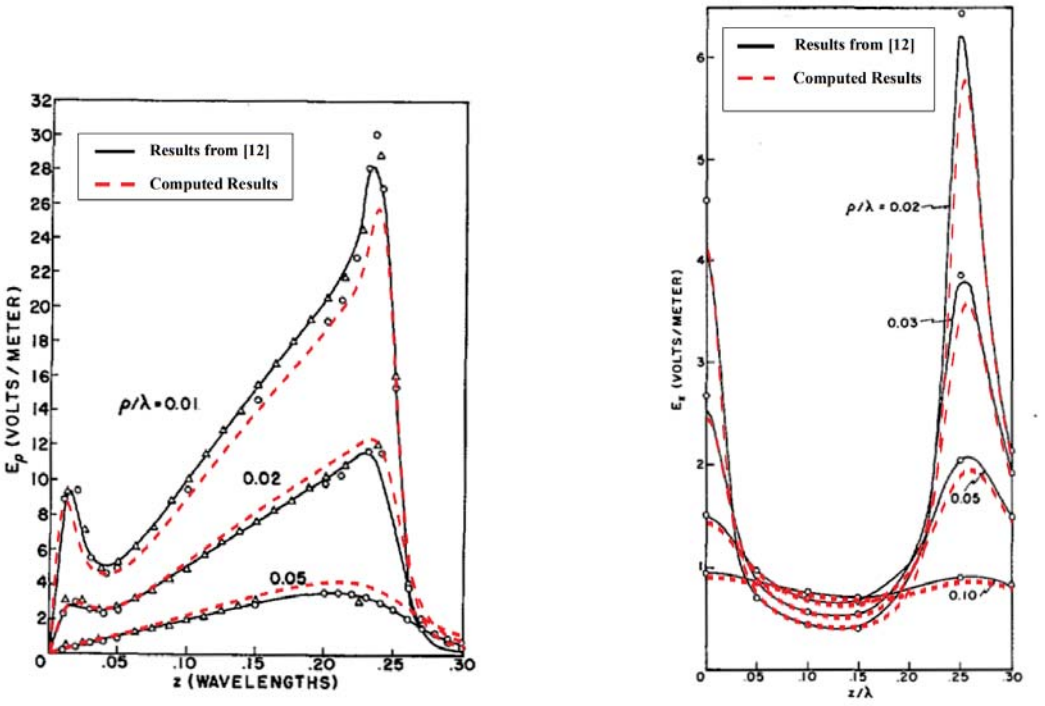

(a) (b)

Fig. 2.5: Comparison plot of the computed near-field components with [12] (a) E_ρ w.r.t. z/λ (b) E_z w.r.t. z/λ

as noted in the literature [13, 14]. King and Wu [13] have predicted a $(\ln \rho/a)$ dependence of E_z near the dipole surface. These data very closely approximate such dependence in the central region $(z/\lambda \approx 0.125)$. Near the gap and ends of the antenna, however, the curves show crossover and, therefore, a departure from the $(\ln \rho/a)$ dependence. Note that in the central region, the tangential component E_z has a $(1/\rho)$ dependence for large ρ/a. Therefore, E_z, as a function of ρ, increases to a maximum value (at about $\rho = 0.1\lambda$) and then decreases monotonically. On the other hand, for $z = 0, 0.25\lambda$, E_z decreases monotonically as a function of ρ.

Fig. 2.6 shows the phase plot for the radial and tangential components of near-fields. Both the results obtained from Method 1 and Method 2 give the same results. Fig.

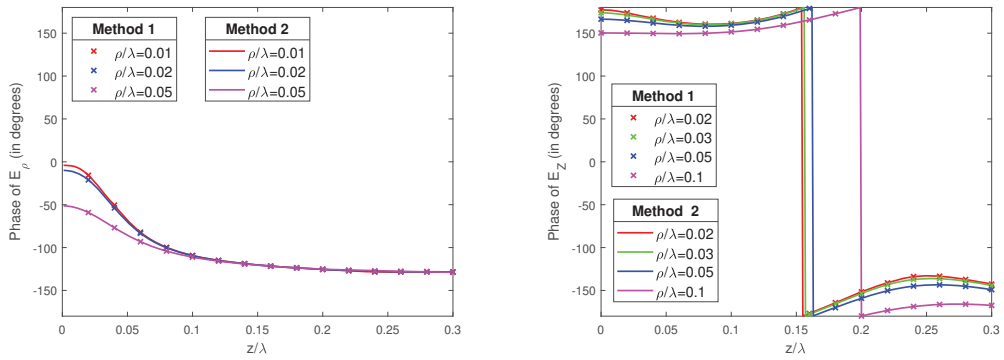

(a) (b)

Fig. 2.6: Phase Plot of the Near-field components of a center-fed half dipole (radius = 0.005λ) (a) E_ρ w.r.t. z/λ (b) E_z w.r.t. z/λ

2.6(a) shows the phase of the radial fields E_ρ in degrees computed for ρ/λ values, 0.01, 0.02, and 0.05 and Fig. 2.6(b) illustrates the phase of the tangential fields E_z components in degrees, computed for ρ/λ values, 0.02, 0.03, 0.05, and 0.1.

Fig. 2.7 shows the variation of the E_ρ and E_z components when the number of segments N is varied from 24 to 100 for $\rho/\lambda = 0.02$. It can be observed from the plots that the magnitude of both E_ρ and E_z are converging with increasing N.

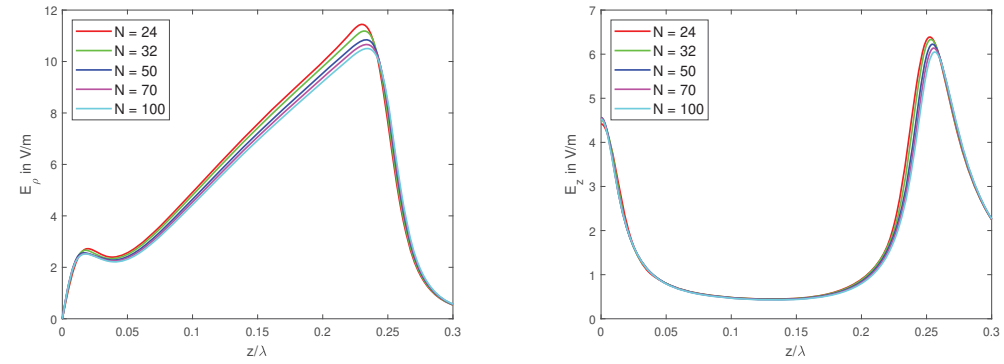

(a) (b)

Fig. 2.7: Plot of the computed near-field components for different no. of segments for $\rho/\lambda = 0.02$ (a) E_ρ w.r.t. z/λ (b) E_z w.r.t. z/λ